

New physics and tau $g - 2$ using LHC heavy ion collisions

Lydia Beresford^{1,*} and Jesse Liu^{1,2,†}

¹*Department of Physics, University of Oxford, Oxford OX1 3RH, UK*

²*Department of Physics, University of Chicago, Chicago IL 60637, USA*

The anomalous magnetic moment of the tau lepton $a_\tau = (g_\tau - 2)/2$ strikingly evades measurement, but is highly sensitive to new physics such as compositeness or supersymmetry. We propose using ultraperipheral heavy ion collisions at the LHC to probe modified magnetic δa_τ and electric dipole moments δd_τ . We introduce a suite of one electron/muon plus track(s) analyses, leveraging the exceptionally clean photon fusion $\gamma\gamma \rightarrow \tau\tau$ events to reconstruct both leptonic and hadronic tau decays sensitive to $\delta a_\tau, \delta d_\tau$. Assuming 10% systematic uncertainties, the current 2 nb^{-1} lead-lead dataset could already provide constraints of $-0.0080 < a_\tau < 0.0046$ at 68% CL. This surpasses 15 year old lepton collider precision by a factor of three while opening novel avenues to new physics.

I. INTRODUCTION

Precision measurements of electromagnetic couplings are foundational tests of quantum electrodynamics (QED) and powerful probes of beyond the Standard Model (BSM) physics. The electron anomalous magnetic moment $a_e = \frac{1}{2}(g_e - 2)$ is among the most precisely known quantities in nature [1–5]. The muon counterpart a_μ is measured to 10^{-7} precision [6] and reports a $3 - 4\sigma$ tension from SM predictions [7, 8]. This may indicate new physics [9–12], to be clarified at Fermilab [13] and J-PARC [14]. Measuring a_ℓ generically tests lepton compositeness [15], while supersymmetry at energy scales M_S induces radiative corrections $\delta a_\ell \sim m_\ell^2/M_S^2$ for leptons with mass m_ℓ [9]. Thus the tau τ can be $m_\tau^2/m_\mu^2 \sim 280$ times more sensitive to BSM physics than a_μ .

However, a_τ continues to evade measurement because the short tau proper lifetime $\sim 10^{-13}$ s precludes use of spin precession methods [6]. The most precise single-experiment measurement a_τ^{exp} is from DELPHI [16, 17] at the Large Electron Positron Collider (LEP), but is remarkably an order of magnitude away from the theoretical central value $a_{\tau, \text{SM}}^{\text{pred}}$ predicted to 10^{-5} precision [18]

$$a_\tau^{\text{exp}} = -0.018(17), \quad a_{\tau, \text{SM}}^{\text{pred}} = 0.001\,177\,21(5). \quad (1)$$

The poor constraints on a_τ present striking room for BSM physics, especially given other lepton sector tensions [19–26], and motivate new experimental strategies.

This Letter proposes a suite of analyses to probe a_τ using heavy ion beams at the LHC. We leverage ultraperipheral collisions (UPC) where only the electromagnetic fields surrounding lead (Pb) ions interact. Tau pairs are produced from photon fusion $\text{PbPb} \rightarrow \text{Pb}(\gamma\gamma \rightarrow \tau\tau)\text{Pb}$, illustrated in Fig. 1, whose sensitivity to a_τ was suggested in 1991 [27]. We introduce the strategy crucial for experimental realization and importantly show that the currently recorded dataset could already surpass LEP precision. The LHC cross-section enjoys a Z^4 enhancement ($Z = 82$ for Pb), with over one million $\gamma\gamma \rightarrow \tau\tau$ events produced to date. Existing proposals using lepton beams require future datasets (Belle-II) or proposed facilities (CLIC, LHeC) [28–34], while LHC studies focus on high luminosity proton beams [35–40]. No LHC

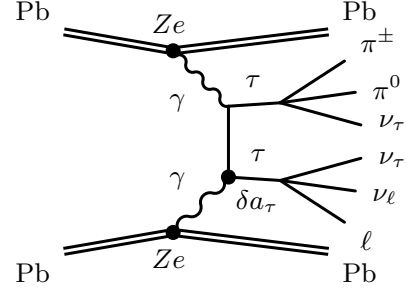


FIG. 1. Pair production of tau leptons τ from ultraperipheral lead ion (Pb) collisions in two of the most common decay modes: $\pi^\pm \pi^0 \nu_\tau$ and $\ell \nu_\ell \nu_\tau$. New physics can modify tau-photon couplings affecting the magnetic moment by δa_τ .

analysis of $\gamma\gamma \rightarrow \tau\tau$ exists as the taus have insufficient momentum for ATLAS/CMS to record or reconstruct.

Our proposal overcomes these obstructions in the clean UPC events [41], enabling selection of individual tracks from tau decays with no other detector activity akin to LEP [16]. We exploit recent advances in low momentum electron/muon identification [42–44] to suppress hadronic backgrounds. We then present a shape analysis sensitive to interfering SM and BSM amplitudes to enhance a_τ constraints. Our strategy also probes tau electric dipole moments d_τ induced by charge-parity (CP) violating new physics. This opens key new directions in the heavy ion program amid reviving interest in photon collisions [45–47] for light-by-light scattering [48–51], standard candle processes [52–56], and BSM dynamics [57–67].

II. EFFECTIVE THEORY & PHOTON FLUX

The anomalous τ magnetic moment $a_\tau = (g_\tau - 2)/2$ is defined by the spin-magnetic Hamiltonian $-\boldsymbol{\mu}_\tau \cdot \mathbf{B} = -(g_\tau e/2m_\tau) \mathbf{S} \cdot \mathbf{B}$. In the Lagrangian formulation of QED, electromagnetic moments arise from the spinor tensor $\sigma^{\mu\nu} = i[\gamma^\mu, \gamma^\nu]/2$ structure of the fermion current interacting with the photon field strength $F_{\mu\nu}$

$$\mathcal{L} = \frac{1}{2} \bar{\tau}_L \sigma^{\mu\nu} \left(a_\tau \frac{e}{2m_\tau} - i d_\tau \gamma_5 \right) \tau_R F_{\mu\nu}. \quad (2)$$

Here, γ^5 satisfies the anticommutator $\{\gamma^5, \gamma^\mu\} = 0$, and $\tau_{L,R}$ are tau spinors with L,R denoting chirality.

To introduce BSM modifications of a_τ and d_τ , we use SM effective field theory (SMEFT) [68]. This assumes the scale of BSM physics Λ is much higher than the probe momentum transfers q i.e., $q^2 \ll \Lambda^2$. At scale q , two dimension-six operators in the Warsaw basis [69] modify a_τ and d_τ at tree level, as discussed in Ref. [68]

$$\mathcal{L}' = (\bar{L}_\tau \sigma^{\mu\nu} \tau_R) H \left[\frac{C_{\tau B}}{\Lambda^2} B_{\mu\nu} + \frac{C_{\tau W}}{\Lambda^2} W_{\mu\nu} \right]. \quad (3)$$

Here, $B_{\mu\nu}$ and $W_{\mu\nu}$ are the $U(1)_Y$ and $SU(2)_L$ field strengths, H (L_τ) is the Higgs (tau lepton) doublet, and C_i are dimensionless, complex Wilson coefficients. We fix $C_{\tau W} = 0$ to parameterize the two modified moments ($\delta a_\tau, \delta d_\tau$) using two real parameters ($|C_{\tau B}|/\Lambda^2, \varphi$) [33]

$$\delta a_\tau = \frac{2m_\tau}{e} \frac{|C_{\tau B}|}{M} \cos \varphi, \quad \delta d_\tau = \frac{|C_{\tau B}|}{M} \sin \varphi, \quad (4)$$

where φ is the complex phase of $C_{\tau B}$, we define $M = \Lambda^2/(\sqrt{2}v \cos \theta_W)$, θ_W is the electroweak Weinberg angle, and $v = 246$ GeV.

In the SM, pair production of electrically charged particles X from photon fusion $\gamma\gamma \rightarrow XX$ have analytic cross-sections $\sigma_{\gamma\gamma \rightarrow XX}$ [64, 70, 71]. For BSM variations, we employ the flavour-general SMEFTSIM package [72], which implements Eq. (3) in FEYNRULES [73]. This allows a direct interface with MADGRAPH 2.6.5 [74, 75] for cross-section calculation and Monte Carlo simulation. To model interference between SM and BSM diagrams, we generate $\gamma\gamma \rightarrow \tau\tau$ events with up to two BSM couplings $C_{\tau B}$ in the matrix element.

Turning to the source of photons, these are emitted coherently from electromagnetic fields surrounding the ultrarelativistic ions, which is known as the equivalent photon approximation [76]. We follow the MADGRAPH implementation in Ref. [77], which assumes the LHC exclusive cross-section $\sigma_{\gamma\gamma \rightarrow XX}^{(\text{PbPb})}$ is factorized into a convolution of $\sigma_{\gamma\gamma \rightarrow XX}$ with the ion photon fluxes $n(x)$

$$\sigma_{\gamma\gamma \rightarrow XX}^{(\text{PbPb})} = \int dx_1 dx_2 n(x_1) n(x_2) \sigma_{\gamma\gamma \rightarrow XX}, \quad (5)$$

where $x_i = E_i/E_{\text{beam}}$ is the ratio of the emitted photon energy E_i from ion i with beam energy E_{beam} . In this factorized prescription, $n(x)$ assumes an analytic form from classical field theory [77, 78]

$$n(x) = \frac{2Z^2\alpha}{x\pi} \left\{ \bar{x} K_0(\bar{x}) K_1(\bar{x}) - \frac{\bar{x}^2}{2} [K_1^2(\bar{x}) - K_0^2(\bar{x})] \right\}, \quad (6)$$

where $\bar{x} = xm_N b_{\text{min}}$, m_N is the nucleon mass $m_N = 0.9315$ GeV, and $Z = 82$ for Pb. We set the minimum impact parameter b_{min} to be the nuclear radius $b_{\text{min}} = R_A \simeq 1.2A^{1/3}$ fm $= 6.09A^{1/3}$ GeV $^{-1}$, where $A = 208$ is the mass number of Pb used at the LHC. We use Ref. [79] to numerically evaluate the modified Bessel functions of the second kind of first K_0 and second K_1 order.

We modify MADGRAPH to use the photon flux Eq. (6) for evaluating $\sigma_{\gamma\gamma \rightarrow XX}^{(\text{PbPb})}$. This prescription neglects a non-factorizable term in Eq. (5), which models the probability of hadronic interactions $P_{|\mathbf{b}_1 - \mathbf{b}_2|}$, where \mathbf{b}_i is the impact parameter of ion i . The SUPERCHIC 3.02 [80] program includes a complete treatment of $P_{|\mathbf{b}_1 - \mathbf{b}_2|}$, along with nuclear overlap and thickness. Using this, we validate that these simplifications in MADGRAPH do not majorly impact distributions relevant for this work, namely tau p_T . We generate 3 million $\gamma\gamma \rightarrow \tau\tau$ events for each coupling variation at $\sqrt{s_{\text{NN}}} = 5.02$ TeV. For the SM, we find $\sigma_{\gamma\gamma \rightarrow \tau\tau}^{(\text{PbPb})} = 5.7 \times 10^5$ nb. To improve generator statistics, we impose $p_T^\tau > 3$ GeV in MADGRAPH, which has a 21% efficiency. Due to destructive interference, $\sigma_{\gamma\gamma \rightarrow \tau\tau}^{(\text{PbPb})}$ falls to a minimum of 4.7×10^5 nb at $\delta a_\tau \simeq -0.04$ before returning to 5.7×10^5 nb at $\delta a_\tau \simeq -0.09$. Further validation of these effects is in Appendix A. We employ PYTHIA 8.230 [81] for decay, shower and hadronization, then use DELPHES 3.4.1 [82] for detector emulation.

III. PROPOSED ANALYSES

To record $\gamma\gamma \rightarrow \tau\tau$ events, dedicated UPC triggers are crucial for our proposal. With no other detector activity, the ditau system receives negligible transverse boost and each tau p_T reaches a few to tens of GeV at most. Taus always decay to a neutrino ν_τ , which further dilutes the visible momenta, rendering usual hadronic tau triggers $p_T^{\text{jet}} \gtrsim 20$ GeV unfeasible [83, 84]. However, UPC events without pileup enable exceptionally low trigger thresholds by vetoing large sums over calorimeter transverse energy deposits $\sum E_T < 50$ GeV [51]. Other minimum bias triggers are also possible [85, 86]. A recent UPC dimuon analysis additionally requires at least one track and no explicit p_T requirement for the trigger muon [56]. The light-by-light observation also considers ultralow $E_T > 1$ GeV calorimeter cluster thresholds at trigger level [51], which can similarly benefit electrons.

We design our event selection around two objectives. First, we consider standard objects already deployed by ATLAS/CMS to efficiently reconstruct tau decays with the following branching fractions [17]:

$$\mathcal{B}(\tau^\pm \rightarrow \ell^\pm \nu_\ell \nu_\tau) = 35\%, \quad (7)$$

$$\mathcal{B}(\tau^\pm \rightarrow \pi^\pm \nu_\tau + \text{neutral pions}) = 45.6\%, \quad (8)$$

$$\mathcal{B}(\tau^\pm \rightarrow \pi^\pm \pi^\mp \pi^\pm \nu_\tau + \text{neutral pions}) = 19.4\%. \quad (9)$$

We develop signal regions (SR) targeting these decays based on expected signal rate and background mitigation strategies. We impose the lowest trigger and reconstruction thresholds $p_T^{e/\mu} > 4.5/3$ GeV, $|\eta_{e/\mu}| < 2.5/2.4$ supported by ATLAS/CMS [42, 43]. Second, we optimize sensitivity to different couplings $\delta a_\tau, \delta d_\tau$, where interfering SM and BSM amplitudes impact tau kinematics, which propagates to e.g. lepton p_T .

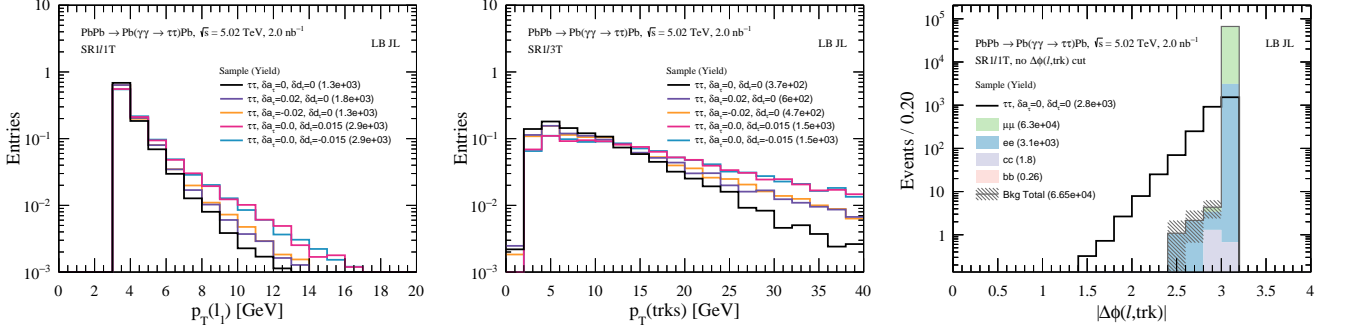


FIG. 2. Distributions of lepton p_T in SR1l1T (left) and the 3-track system p_T in SR1l3T (center) for benchmark signals with various $\delta a_\tau, \delta d_\tau$ couplings. These are normalized to unit integral to illustrate shape changes with varying $\delta a_\tau, \delta d_\tau$. The lepton–track azimuthal angle $|\Delta\phi(\ell, \text{trk})|$ in SR1l1T (right) is shown for backgrounds (filled) and signal $\delta a_\tau = \delta d_\tau = 0$ (line), illustrating powerful discrimination against dilepton processes.

Dilepton analysis. Requiring two leptons is expected to give the highest signal-to-background S/B , with half being different flavor $e\mu$ free of $ee/\mu\mu$ backgrounds. But even using low $p_T^{e/\mu}$ thresholds, we find insufficient signal yields at 2 nb^{-1} to pursue this further.

1 lepton + 1 track analysis (SR1l1T). This requires exactly 1 lepton and 1 other track that is not ‘matched’ to the lepton (the matched track is the highest p_T track with $\Delta R(\ell, \text{track}) < 0.02$). Tracks must satisfy the standard requirements $p_T^{\text{track}} > 500 \text{ MeV}$ and $|\eta^{\text{track}}| < 2.5$. This topology targets the high branching ratio of the single charged pion decay mode and background suppression from lepton identification. The track also recovers events failing the dilepton analysis, in which a lepton is too soft to be reconstructed. We divide this SR into two bins $p_T^{e/\mu} \in [\leq 6], [> 6] \text{ GeV}$ to exploit shape differences shown in Fig. 2 (left). We require nonplanar lepton–track system $|\Delta\phi(\ell, \text{trk})| < 3$ to suppress back-to-back $ee/\mu\mu$ processes, as demonstrated in Fig. 2 (right). We veto invariant masses $m_{\ell, \text{trk}} \notin [3, 3.2], [9, 11] \text{ GeV}$ to reject dilepton decays of J/ψ and Υ resonances.

1 lepton + multitrack analysis (SR1l2/3T). We augment the previous analysis with 3 non-lepton-matched tracks. This targets the distinctive 3 charged pion decay. We also construct an orthogonal 2 tracks SR to recover misreconstructed 3-pion decays. The non-lepton-matched tracks are used to define the tau candidate as the vectorial sum of the tracks $p_\tau^{\text{tracks}} = \sum_i p_i^{\text{track}}$, whose p_T distribution is shown in Fig. 2 (center) for SR1l3T. We find removing lepton identification significantly increases hadronic backgrounds.

Leptonic backgrounds are dominated by dielectron/dimuon production $\gamma\gamma \rightarrow \ell\ell, \ell \in [e, \mu]$. The single flavor cross-section is sizable $\sigma_{\gamma\gamma \rightarrow \ell\ell}^{(\text{PbPb})} = 4.2 \times 10^5 \text{ nb}$, which includes a generator level $|\eta_\ell| < 2.5$ requirement. The back-to-back leptons are suppressed by the $|\Delta\phi_{\ell\ell}| < 3$ requirement, which we verify by generating 1 million events per flavor. Photon radiation from leptons $\ell \rightarrow \ell\gamma$ is only expected to modify the tails marginally. Track impact parameters exploiting displaced tau decays

could further suppress this background.

Hadronic backgrounds arise from diquark production $\gamma\gamma \rightarrow q\bar{q}$ and we generate 1 million events for each of the 5 flavors. For $q \in [u, d, s]$ assuming massless quarks gives a cross-section $\sigma_{\gamma\gamma \rightarrow u\bar{u}}^{(\text{PbPb})}(d\vec{d}, s\vec{s}) = 3.0 \times 10^5 (1.9 \times 10^4) \text{ nb}$. Parton showering produces more tracks than tau decays, which we suppress using lepton isolation and requiring no more than 4 tracks at most. For $q \in [c, b]$, heavy flavor B and D mesons undergo semileptonic decays e.g. $D \rightarrow \pi^0 \ell\nu$. The default MADGRAPH parameters assume massless charm quarks (which is conservative as a finite mass decreases cross-sections), yielding $\sigma_{\gamma\gamma \rightarrow c\bar{c}}^{(\text{PbPb})} = 3.0 \times 10^5 \text{ nb}$. Bottom quarks assume finite mass resulting in a smaller cross-section $\sigma_{\gamma\gamma \rightarrow b\bar{b}}^{(\text{PbPb})} = 1.5 \times 10^3 \text{ nb}$. The leptonic branching fraction $D \rightarrow \pi^0 \ell\nu$ is of order a few percent so is under control, and is further suppressed by isolation.

Smaller potential backgrounds include $\gamma\gamma \rightarrow WW$ but the cross-section $\sigma_{\gamma\gamma \rightarrow WW}^{(\text{PbPb})} = 14 \text{ pb}$ implies this is safely neglected. Exchange of digluon color singlets (Pomerons) also contributes to diquark backgrounds. These involve strong interactions and as the binding energy per nucleon is very small $\sim 8 \text{ MeV}$ [77], the Pb ions emit more neutrons than QED processes, which can be vetoed by the Zero Degree Calorimeter [87]. Soft survival for Pomeron exchange is also lower [77], which gives greater activity in the calorimeter and tracker, and are suppressed by our stringent exclusivity requirements.

Systematic uncertainties require LHC collaborations to reliably quantify, but we discuss expected sources and suggest control strategies. Experimental systematics from current UPC PbPb dimuon measurements have systematics of around 10%, dominated by luminosity and trigger [56]. Systematics from lepton reconstruction are p_T^ℓ -dependent and thus sensitive to δa_τ . These are most significant at low p_T , but are currently determined in high luminosity proton collisions with challenging backgrounds from fakes [88, 89], and could be better controlled using clean $\gamma\gamma \rightarrow \ell\ell$ events.

Theoretical uncertainties are expected to be dominated

by modeling of the photon flux, nuclear form factors and nucleon dissociation. Fortunately, these initial state effects are independent of QED process and final state. So, experimentalists could use a control sample of $\gamma\gamma \rightarrow \ell\ell$ events to constrain these universal nuclear systematics or eliminate them in a ratio analysis with dileptons $\sigma_{\gamma\gamma \rightarrow \tau\tau}^{(\text{PbPb})}/\sigma_{\gamma\gamma \rightarrow \ell\ell}^{(\text{PbPb})}$. Hadronic backgrounds are susceptible to uncertainties from modeling the parton shower, but are subdominant given $S/B \gg 1$ in our analyses.

IV. RESULTS & DISCUSSION

We now estimate the sensitivity of our analyses to modified tau moments $\delta a_\tau, \delta d_\tau$. Assuming the observed data correspond to the SM expectation, we calculate

$$\chi^2 = \frac{(S_{\text{SM}+\text{BSM}} - S_{\text{SM}})^2}{B + S_{\text{SM}+\text{BSM}} + (\zeta_s S_{\text{SM}+\text{BSM}})^2 + (\zeta_b B)^2}. \quad (10)$$

Here, B is the background rate, and S_{SM} ($S_{\text{SM}+\text{BSM}}$) is the signal yield assuming SM couplings (nonzero $\delta a_\tau, \delta d_\tau$). At $\mathcal{L} = 2 \text{ nb}^{-1}$, we find $S_{\text{SM}} = 1280, B = 7.6$ for SR1l1T before binning in p_T^ℓ ; $S_{\text{SM}} = 520, B = 15$ for SR1l2T; $S_{\text{SM}} = 370, B = 4$ for SR1l3T. We denote the relative signal (background) systematic uncertainties by ζ_s (ζ_b) and study $\zeta_s = \zeta_b \in [5\%, 10\%]$ as benchmarks. For simplicity, we assume identical ζ_s for all couplings, and combine the four SRs (SR1l1T has two p_T^ℓ bins) using $\chi^2 = \sum \chi_{\text{SR}}^2$ assuming uncorrelated systematics. We define the 68% CL (95% CL) regions as couplings satisfying $\chi^2 < 1$ ($\chi^2 < 3.84$). Appendix B details cutflows for signals and backgrounds, and χ^2 distributions.

Figure 3 summarizes our projected $a_\tau = a_{\tau, \text{SM}}^{\text{pred}} + \delta a_\tau$ constraints (green) compared with existing measurements and predictions. Assuming the current dataset $\mathcal{L} = 2 \text{ nb}^{-1}$ with 10% systematics, we find $-0.0080 < a_\tau < 0.0046$ at 68% CL, surpassing DELPHI precision [16] (blue) by a factor of three. Negative values of δa_τ are more difficult to constrain given destructive interference. We estimate prospects assuming halved systematics giving $-0.0022 < a_\tau < 0.0037$ (68% CL). A tenfold dataset increase for the High Luminosity LHC (HL-LHC) reduces this to $-0.00044 < a_\tau < 0.0032$ (68% CL), an order of magnitude improvement beyond DELPHI. Importantly, these advances start constraining the sign of a_τ and becomes comparable to the predicted SM central value for the first time.

Such precision indirectly probes BSM physics. In nature, compositeness can induce large and negative magnetic moments e.g. the neutron [17]. As a benchmark, we fix $C_{\tau B} = -1, C_{\tau W} = 0, \delta d_\tau = 0$ in Eq. 3 to recast the DELPHI limit into a 95% CL exclusion of $\Lambda < 140 \text{ GeV}$. The orange line in Fig. 3 shows $140 < \Lambda < 250 \text{ GeV}$, where our 2 nb^{-1} , 10% systematics proposal has 95% CL sensitivity, surpassing DELPHI by 110 GeV. In suitable ultraviolet completions of SMEFT with composite leptons, one can interpret Λ as the confinement scale of tau

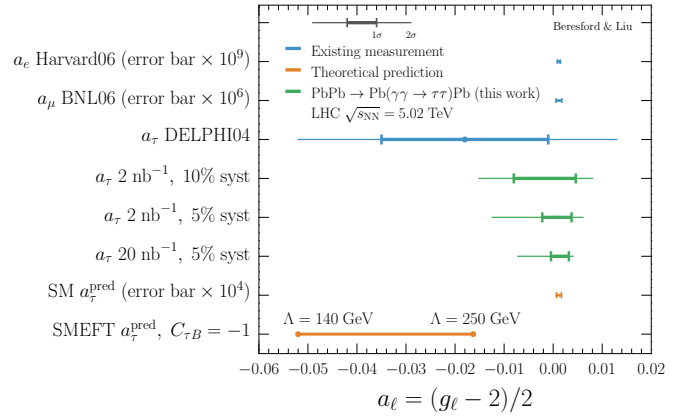


FIG. 3. Summary of lepton anomalous magnetic moments $a_\ell = (g_\ell - 2)/2$. Existing single-experiment measurements of a_e [1], a_μ [6], and a_τ [16] are in blue. Our benchmark projections (green) assume 2 nb^{-1} and 20 nb^{-1} for 5% and 10% systematic uncertainties. For visual clarity, we inflate 1σ error bars on a_e (a_μ) measurements by 10^9 (10^6), and 10^4 for the SM prediction a_τ^{pred} (orange) [18]. Collider constraints have thick (thin) lines denoting 68% CL, 1σ (95% CL, $\sim 2\sigma$). The SMEFT predictions [68, 69] from Eq. (4) with $C_{\tau B} = -1$ displays BSM scales $140 < \Lambda < 250 \text{ GeV}$ (thick orange).

substructure [15]. Nonetheless, our analyses are highly model-independent and we defer sensitivity to other BSM scenarios for future work. It would be interesting to correlate a_τ with models that simultaneously explain tensions in a_e and a_μ [19–21] or B -physics lepton universality tests [22–26].

Lepton electric dipole moments are highly suppressed in the SM, arising only at four-loop $|d_\tau^{\text{pred}}| \sim (m_\tau/m_e)|d_e^{\text{pred}}| \sim 10^{-33} e \text{ cm}$ [90]. Additional CP violation in the lepton sector can enhance this, such as neutrino mixing [91], or other BSM physics parameterized by φ in Eq. 4. Our projected 95% CL sensitivity on $d_\tau = (e/m_\tau)\delta d_\tau$ is $|d_\tau| < 3.4 \times 10^{-17} e \text{ cm}$, assuming $\delta a_\tau = 0$ with 2 nb^{-1} , 10% systematics. This is an order of magnitude better than DELPHI $|d_\tau| < 3.7 \times 10^{-16} e \text{ cm}$ [16] and competitive with Belle [92].

Our proposal opens numerous avenues for extension. Lowering lepton/track thresholds to increase statistics would enable more optimized differential or multivariate analyses. Recently, ATLAS considered tracks matched to lepton candidates failing quality requirements, allowing $p_T^{\text{track}}(e/\mu) > 1/2 \text{ GeV}$ [44]. Moreover the 500 MeV track threshold is conservative given $p_T^{\text{track}} > 100 \text{ MeV}$ is successfully used in ATLAS [51]. Reconstructing soft calorimeter clusters could enable hadron/electron identification, or using neutral pions to improve tau momentum resolution. Proposed timing detectors may offer more robust particle identification in ATLAS/CMS [93] while ALICE already has such capabilities [94]. Ultimate a_τ precision requires a coordinated worldwide program led by LHC efforts combined with proton-lead collisions at $\sqrt{s_{\text{NN}}} = 8.76 \text{ TeV}$, Relativistic Heavy Ion Collider

(RHIC), and lepton colliders.

To summarize, we proposed a strategy of lepton plus track(s) analyses to surpass LEP constraints on tau electromagnetic moments using heavy ion data already recorded by the LHC. The clean photon collision events provide excellent opportunities to optimize low momentum reconstruction and control systematics further. We encourage LHC collaborations to open these cornerstone measurements and precision pathways to new physics.

Acknowledgements—We thank the hospitality of

the LHC Forward and Diffractive Physics Workshop at CERN, where part of this work began. We are grateful to Luca Ambroz, Bill Balunas, Alan Barr, Mikkel Bjørn, Barak Gruber, Lucian Harland-Lang, Simon Knapen, Santiago Paredes, Hannah Pullen, Hayden Smith, Beojan Stanislaus, Gabija Žemaitytė and Miha Zgubič for helpful discussions. LB is supported by a Junior Research Fellowship at St John’s College, Oxford. JL is supported by an STFC Postgraduate Studentship at Oxford, where this work started, and the Grainger Fellowship.

* lydia.beresford@physics.ox.ac.uk

† jesseliu@uchicago.edu

- [1] B. Odom, D. Hanneke, B. D’Urso, and G. Gabrielse, “New Measurement of the Electron Magnetic Moment Using a One-Electron Quantum Cyclotron,” *Phys. Rev. Lett.* **97**, 030801 (2006).
- [2] D. Hanneke, S. Fogwell Hoogerheide, and G. Gabrielse, “Cavity Control of a Single-Electron Quantum Cyclotron: Measuring the Electron Magnetic Moment,” *Phys. Rev. A* **83**, 052122 (2011), [arXiv:1009.4831 \[physics.atom-ph\]](#).
- [3] R. Bouchendira, P. Cladé, S. Guellati-Khélifa, F. Nez, and F. Biraben, “New Determination of the Fine Structure Constant and Test of the Quantum Electrodynamics,” *Phys. Rev. Lett.* **106**, 080801 (2011).
- [4] T. Aoyama, M. Hayakawa, T. Kinoshita, and M. Nio, “Tenth-Order QED Contribution to the Electron $g-2$ and an Improved Value of the Fine Structure Constant,” *Phys. Rev. Lett.* **109**, 111807 (2012), [arXiv:1205.5368 \[hep-ph\]](#).
- [5] R. H. Parker, C. Yu, W. Zhong, B. Estey, and H. Müller, “Measurement of the fine-structure constant as a test of the Standard Model,” *Science* **360**, 191–195 (2018).
- [6] G. W. Bennett *et al.* (Muon $g-2$), “Final Report of the Muon E821 Anomalous Magnetic Moment Measurement at BNL,” *Phys. Rev. D* **73**, 072003 (2006), [arXiv:hep-ex/0602035 \[hep-ex\]](#).
- [7] T. Aoyama, M. Hayakawa, T. Kinoshita, and M. Nio, “Complete Tenth-Order QED Contribution to the Muon $g-2$,” *Phys. Rev. Lett.* **109**, 111808 (2012), [arXiv:1205.5370 \[hep-ph\]](#).
- [8] A. Keshavarzi, D. Nomura, and T. Teubner, “Muon $g-2$ and $\alpha(M_Z^2)$: a new data-based analysis,” *Phys. Rev. D* **97**, 114025 (2018), [arXiv:1802.02995 \[hep-ph\]](#).
- [9] Stephen P. Martin and James D. Wells, “Muon Anomalous Magnetic Dipole Moment in Supersymmetric Theories,” *Phys. Rev. D* **64**, 035003 (2001), [arXiv:hep-ph/0103067 \[hep-ph\]](#).
- [10] Andrzej Czarnecki and William J. Marciano, “The Muon anomalous magnetic moment: A Harbinger for ‘new physics’,” *Phys. Rev. D* **64**, 013014 (2001), [arXiv:hep-ph/0102122 \[hep-ph\]](#).
- [11] K. Hagiwara, R. Liao, A. D. Martin, D. Nomura, and T. Teubner, “ $(g-2)_\mu$ and $\alpha(M_Z^2)$ re-evaluated using new precise data,” *J. Phys. G* **38**, 085003 (2011), [arXiv:1105.3149 \[hep-ph\]](#).
- [12] M. Adeel Ajaib, B. Dutta, T. Ghosh, I. Gogoladze, and Q. Shafi, “Neutralinos and sleptons at the LHC in light of muon $(g-2)_\mu$,” *Phys. Rev. D* **92**, 075033 (2015), [arXiv:1505.05896 \[hep-ph\]](#).
- [13] J. Grange *et al.* (Muon $g-2$), “Muon ($g-2$) Technical Design Report,” (2015), [arXiv:1501.06858 \[physics.ins-det\]](#).
- [14] M. Abe *et al.*, “A New Approach for Measuring the Muon Anomalous Magnetic Moment and Electric Dipole Moment,” (2019), [arXiv:1901.03047 \[physics.ins-det\]](#).
- [15] D. J. Silverman and G. L. Shaw, “Limits on the Composite Structure of the Tau Lepton and Quarks From Anomalous Magnetic Moment Measurements in e^+e^- Annihilation,” *Phys. Rev. D* **27**, 1196 (1983).
- [16] J. Abdallah *et al.* (DELPHI), “Study of tau-pair production in photon-photon collisions at LEP and limits on the anomalous electromagnetic moments of the tau lepton,” *Eur. Phys. J. C* **35**, 159–170 (2004), [arXiv:hep-ex/0406010 \[hep-ex\]](#).
- [17] M. Tanabashi *et al.* (Particle Data Group), “Review of Particle Physics,” *Phys. Rev. D* **98**, 030001 (2018).
- [18] S. Eidelman and M. Passera, “Theory of the tau lepton anomalous magnetic moment,” *Mod. Phys. Lett. A* **22**, 159–179 (2007), [arXiv:hep-ph/0701260 \[hep-ph\]](#).
- [19] B. Dutta and Y. Mimura, “Electron $g-2$ with flavor violation in MSSM,” *Phys. Lett. B* **790**, 563–567 (2019), [arXiv:1811.10209 \[hep-ph\]](#).
- [20] H. Davoudiasl and W. J. Marciano, “Tale of two anomalies,” *Phys. Rev. D* **98**, 075011 (2018), [arXiv:1806.10252 \[hep-ph\]](#).
- [21] M. Bauer, M. Neubert, S. Renner, M. Schnubel, and A. Thamm, “Axion-like particles, lepton-flavor violation and a new explanation of a_μ and a_e ,” (2019), [arXiv:1908.00008 \[hep-ph\]](#).
- [22] LHCb Collaboration, “Measurement of the ratio of branching fractions $\mathcal{B}(\bar{B}^0 \rightarrow D^{*+}\tau^-\bar{\nu}_\tau)/\mathcal{B}(\bar{B}^0 \rightarrow D^{*+}\mu^-\bar{\nu}_\mu)$,” *Phys. Rev. Lett.* **115**, 111803 (2015), [Erratum: *Phys. Rev. Lett.* **115**, no.15, 159901(2015)], [arXiv:1506.08614 \[hep-ex\]](#).
- [23] Belle Collaboration, “Measurement of $\mathcal{R}(D)$ and $\mathcal{R}(D^*)$ with a semileptonic tagging method,” (2019), [arXiv:1904.08794 \[hep-ex\]](#).
- [24] B. Allanach, F. S. Queiroz, A. Strumia, and S. Sun, “ Z' models for the LHCb and $g-2$ muon anomalies,” *Phys. Rev. D* **93**, 055045 (2016), [Erratum: *Phys. Rev. D* **95**, no.11, 119902(2017)], [arXiv:1511.07447 \[hep-ph\]](#).
- [25] S. Di Chiara, A. Fowlie, S. Fraser, C. Marzo, L. Marzola, M. Raidal, and C. Spethmann, “Minimal flavor-changing Z' models and muon $g-2$ after the R_{K^*} measurement,” *Nucl. Phys. B* **923**, 245–257 (2017), [arXiv:1704.06200 \[hep-ph\]](#).
- [26] A. Biswas and A. Shaw, “Reconciling dark matter, $R_{K^{(*)}}$

- anomalies and $(g - 2)_\mu$ in an $L_\mu - L_\tau$ scenario,” *JHEP* **05**, 165 (2019), [arXiv:1903.08745 \[hep-ph\]](#).
- [27] F. del Aguila, F. Cornet, and J. I. Illana, “The possibility of using a large heavy-ion collider for measuring the electromagnetic properties of the tau lepton,” *Physics Letters B* **271**, 256 – 260 (1991).
- [28] M. Koksál, A. A. Billur, A. Gutiérrez-Rodríguez, and M. A. Hernández-Ruíz, “Model-independent sensitivity estimates for the electromagnetic dipole moments of the τ -lepton at the CLIC,” *Phys. Rev. D* **98**, 015017 (2018), [arXiv:1804.02373 \[hep-ph\]](#).
- [29] J. N. Howard, A. Rajaraman, R. Riley, and T. M. P. Tait, “The τ Magnetic Dipole Moment at Future Lepton Colliders,” (2018), [arXiv:1810.09570 \[hep-ph\]](#).
- [30] M. Koksál, “Search for the electromagnetic moments of the τ lepton in photon-photon collisions at the LHeC and the FCC-he,” (2018), [arXiv:1809.01963 \[hep-ph\]](#).
- [31] A. Gutiérrez-Rodríguez, M. Koksál, A. A. Billur, and M. A. Hernández-Ruíz, “Feasibility at the LHC, FCC-he and CLIC for sensitivity estimates on anomalous τ -lepton couplings,” (2019), [arXiv:1903.04135 \[hep-ph\]](#).
- [32] M. Fael, L. Mercolli, and M. Passera, “Towards a determination of the tau lepton dipole moments,” *Nucl. Phys. Proc. Suppl.* **253-255**, 103–106 (2014), [arXiv:1301.5302 \[hep-ph\]](#).
- [33] S. Eidelman, D. Epifanov, M. Fael, L. Mercolli, and M. Passera, “ τ dipole moments via radiative leptonic τ decays,” *JHEP* **03**, 140 (2016), [arXiv:1601.07987 \[hep-ph\]](#).
- [34] X. Chen and Y. Wu, “Search for the Electric Dipole Moment and anomalous magnetic moment of the tau lepton at tau factories,” (2018), [arXiv:1803.00501 \[hep-ph\]](#).
- [35] M. A. Samuel and G. Li, “How to measure the magnetic moment of the tau lepton,” *International Journal of Theoretical Physics* **33**, 1471–1477 (1994).
- [36] Alper Hayreter and German Valencia, “Constraining τ -lepton dipole moments and gluon couplings at the LHC,” *Phys. Rev. D* **88**, 013015 (2013), [Erratum: *Phys. Rev. D* **91**, no.9, 099902(2015)], [arXiv:1305.6833 \[hep-ph\]](#).
- [37] S. Atag and A. A. Billur, “Possibility of Determining τ Lepton Electromagnetic Moments in $\gamma\gamma \rightarrow \tau^+\tau^-$ Process at the CERN-LHC,” *JHEP* **11**, 060 (2010), [arXiv:1005.2841 \[hep-ph\]](#).
- [38] I. Galon, A. Rajaraman, and T. M. P. Tait, “ $H \rightarrow \tau^+\tau^-\gamma$ as a probe of the τ magnetic dipole moment,” *JHEP* **12**, 111 (2016), [arXiv:1610.01601 \[hep-ph\]](#).
- [39] A. S. Fomin, A. Yu Korchin, A. Stocchi, S. Barsuk, and P. Robbe, “Feasibility of τ -lepton electromagnetic dipole moments measurement using bent crystal at the LHC,” *JHEP* **03**, 156 (2019), [arXiv:1810.06699 \[hep-ph\]](#).
- [40] J. Fu, M. A. Giorgi, L. Henry, D. Marangotto, F. Martínez Vidal, A. Merli, N. Neri, and J. Ruiz Vidal, “Novel Method for the Direct Measurement of the τ Lepton Dipole Moments,” *Phys. Rev. Lett.* **123**, 011801 (2019), [arXiv:1901.04003 \[hep-ex\]](#).
- [41] ATLAS Collaboration, *Back-to-back electron-muon pair in an ultra-peripheral collision recorded with the ATLAS detector*, Tech. Rep. (2018).
- [42] ATLAS Collaboration, “Search for electroweak production of supersymmetric states in scenarios with compressed mass spectra at $\sqrt{s} = 13$ TeV with the ATLAS detector,” *Phys. Rev. D* **97**, 052010 (2018), [arXiv:1712.08119 \[hep-ex\]](#).
- [43] CMS Collaboration, “Search for new physics in events with two soft oppositely charged leptons and missing transverse momentum in proton-proton collisions at $\sqrt{s} = 13$ TeV,” *Phys. Lett. B* **782**, 440–467 (2018), [arXiv:1801.01846 \[hep-ex\]](#).
- [44] ATLAS Collaboration, *Searches for electroweak production of supersymmetric particles with compressed mass spectra in $\sqrt{s} = 13$ TeV pp collisions with the ATLAS detector*, Tech. Rep. ATLAS-CONF-2019-014 (2019).
- [45] K. Piotrkowski, “Tagging two photon production at the CERN LHC,” *Phys. Rev. D* **63**, 071502 (2001), [arXiv:hep-ex/0009065 \[hep-ex\]](#).
- [46] M. G. Albrow *et al.* (FP420 R & D), “The FP420 R & D Project: Higgs and New Physics with forward protons at the LHC,” *JINST* **4**, T10001 (2009), [arXiv:0806.0302 \[hep-ex\]](#).
- [47] J. de Favereau de Jeneret, V. Lemaitre, Y. Liu, S. Olyn, T. Pierzchala, K. Piotrkowski, X. Rouby, N. Schul, and M. Vander Donckt, “High energy photon interactions at the LHC,” (2009), [arXiv:0908.2020 \[hep-ph\]](#).
- [48] D. d’Enterria and G. G. da Silveira, “Observing light-by-light scattering at the Large Hadron Collider,” *Phys. Rev. Lett.* **111**, 080405 (2013), [Erratum: *Phys. Rev. Lett.* **116**, no.12, 129901(2016)], [arXiv:1305.7142 \[hep-ph\]](#).
- [49] ATLAS Collaboration, “Evidence for light-by-light scattering in heavy-ion collisions with the ATLAS detector at the LHC,” *Nature Phys.* **13**, 852–858 (2017), [arXiv:1702.01625 \[hep-ex\]](#).
- [50] CMS Collaboration, “Evidence for light-by-light scattering and searches for axion-like particles in ultraperipheral PbPb collisions at $\sqrt{s_{NN}} = 5.02$ TeV,” (2018), [arXiv:1810.04602 \[hep-ex\]](#).
- [51] ATLAS Collaboration, “Observation of light-by-light scattering in ultraperipheral Pb+Pb collisions with the ATLAS detector,” *Phys. Rev. Lett.* **123**, 052001 (2019), [arXiv:1904.03536 \[hep-ex\]](#).
- [52] ATLAS Collaboration, “Measurement of the exclusive $\gamma\gamma \rightarrow \mu^+\mu^-$ process in proton-proton collisions at $\sqrt{s} = 13$ TeV with the ATLAS detector,” *Phys. Lett. B* **777**, 303–323 (2018), [arXiv:1708.04053 \[hep-ex\]](#).
- [53] ATLAS Collaboration, “Measurement of exclusive $\gamma\gamma \rightarrow W^+W^-$ production and search for exclusive Higgs boson production in pp collisions at $\sqrt{s} = 8$ TeV using the ATLAS detector,” *Phys. Rev. D* **94**, 032011 (2016), [arXiv:1607.03745 \[hep-ex\]](#).
- [54] CMS Collaboration, “Search for exclusive or semi-exclusive photon pair production and observation of exclusive and semi-exclusive electron pair production in pp collisions at $\sqrt{s} = 7$ TeV,” *JHEP* **11**, 080 (2012), [arXiv:1209.1666 \[hep-ex\]](#).
- [55] CMS Collaboration, “Evidence for exclusive $\gamma\gamma \rightarrow W^+W^-$ production and constraints on anomalous quartic gauge couplings in pp collisions at $\sqrt{s} = 7$ and 8 TeV,” *JHEP* **08**, 119 (2016), [arXiv:1604.04464 \[hep-ex\]](#).
- [56] ATLAS Collaboration, *Measurement of high-mass dimuon pairs from ultraperipheral lead-lead collisions at $\sqrt{s_{NN}} = 5.02$ TeV with the ATLAS detector*, Tech. Rep. ATLAS-CONF-2016-025 (2016).
- [57] E. Chapon, C. Royon, and O. Kepka, “Anomalous quartic $WW\gamma\gamma$, $ZZ\gamma\gamma$, and trilinear $WW\gamma$ couplings in two-photon processes at high luminosity at the LHC,” *Phys. Rev. D* **81**, 074003 (2010), [arXiv:0912.5161 \[hep-ph\]](#).
- [58] S. Fichet, G. von Gersdorff, O. Kepka, B. Lenzi, C. Royon, and M. Saimpert, “Probing new physics in diphoton production with proton tagging at the

- Large Hadron Collider,” *Phys. Rev.* **D89**, 114004 (2014), [arXiv:1312.5153 \[hep-ph\]](#).
- [59] J. Ellis, N. E. Mavromatos, and T. You, “Light-by-Light Scattering Constraint on Born-Infeld Theory,” *Phys. Rev. Lett.* **118**, 261802 (2017), [arXiv:1703.08450 \[hep-ph\]](#).
- [60] S. Knapen, T. Lin, H. K. Lou, and T. Melia, “Searching for Axionlike Particles with Ultraperipheral Heavy-Ion Collisions,” *Phys. Rev. Lett.* **118**, 171801 (2017), [arXiv:1607.06083 \[hep-ph\]](#).
- [61] C. Baldenegro, S. Fichtel, G. von Gersdorff, and C. Royon, “Searching for axion-like particles with proton tagging at the LHC,” *JHEP* **06**, 131 (2018), [arXiv:1803.10835 \[hep-ph\]](#).
- [62] J. Ohnemus, T. F. Walsh, and P. M. Zerwas, “gamma gamma production of nonstrongly interacting SUSY particles at hadron colliders,” *Phys. Lett.* **B328**, 369–373 (1994), [arXiv:hep-ph/9402302 \[hep-ph\]](#).
- [63] N. Schul and K. Piotrkowski, “Detection of two-photon exclusive production of supersymmetric pairs at the LHC,” *Nucl. Phys. Proc. Suppl.* **179–180**, 289–297 (2008), [arXiv:0806.1097 \[hep-ph\]](#).
- [64] L. A. Harland-Lang, C. H. Kom, K. Sakurai, and W. J. Stirling, “Measuring the masses of a pair of semi-invisibly decaying particles in central exclusive production with forward proton tagging,” *Eur. Phys. J.* **C72**, 1969 (2012), [arXiv:1110.4320 \[hep-ph\]](#).
- [65] L. Beresford and J. Liu, “Photon collider search strategy for sleptons and dark matter at the LHC,” (2018), [arXiv:1811.06465 \[hep-ph\]](#).
- [66] L. A. Harland-Lang, V. A. Khoze, M. G. Ryskin, and M. Tasevsky, “LHC Searches for Dark Matter in Compressed Mass Scenarios: Challenges in the Forward Proton Mode,” *JHEP* **04**, 010 (2019), [arXiv:1812.04886 \[hep-ph\]](#).
- [67] R. Bruce *et al.*, “New physics searches with heavy-ion collisions at the LHC,” (2018), [arXiv:1812.07688 \[hep-ph\]](#).
- [68] R. Escribano and E. Masso, “New bounds on the magnetic and electric moments of the tau lepton,” *Phys. Lett.* **B301**, 419–422 (1993).
- [69] B. Grzadkowski, M. Iskrzynski, M. Misiak, and J. Rosiek, “Dimension-Six Terms in the Standard Model Lagrangian,” *JHEP* **10**, 085 (2010), [arXiv:1008.4884 \[hep-ph\]](#).
- [70] S. J. Brodsky, T. Kinoshita, and H. Terazawa, “Two Photon Mechanism of Particle Production by High-Energy Colliding Beams,” *Phys. Rev.* **D4**, 1532–1557 (1971).
- [71] G. Tupper and M. A. Samuel, “ W^+W^- pair production in two-photon collisions and the magnetic moment of the W^\pm bosons,” *Phys. Rev. D* **23**, 1933–1939 (1981).
- [72] I. Brivio, Y. Jiang, and M. Trott, “The SMEFTsim package, theory and tools,” *JHEP* **12**, 070 (2017), [arXiv:1709.06492 \[hep-ph\]](#).
- [73] A. Alloul, N. D. Christensen, C. Degrande, C. Duhr, and B. Fuks, “FeynRules 2.0 - A complete toolbox for tree-level phenomenology,” *Comput. Phys. Commun.* **185**, 2250–2300 (2014), [arXiv:1310.1921 \[hep-ph\]](#).
- [74] J. Alwall, M. Herquet, F. Maltoni, O. Mattelaer, and T. Stelzer, “MadGraph 5 : Going Beyond,” *JHEP* **06**, 128 (2011), [arXiv:1106.0522 \[hep-ph\]](#).
- [75] J. Alwall *et al.*, “The automated computation of tree-level and next-to-leading order differential cross sections, and their matching to parton shower simulations,” *JHEP* **07**, 079 (2014), [arXiv:1405.0301 \[hep-ph\]](#).
- [76] V. M. Budnev, I. F. Ginzburg, G. V. Meledin, and V. G. Serbo, “The Two photon particle production mechanism. Physical problems. Applications. Equivalent photon approximation,” *Phys. Rept.* **15**, 181–281 (1975).
- [77] D. d’Enterria and J.-P. Lansberg, “Study of Higgs boson production and its b anti- b decay in gamma-gamma processes in proton-nucleus collisions at the LHC,” *Phys. Rev.* **D81**, 014004 (2010), [arXiv:0909.3047 \[hep-ph\]](#).
- [78] J. D. Jackson, *Classical electrodynamics; 3rd ed.* (Wiley, New York, NY, 1999).
- [79] S. Zhang and J.M. Jin, *Computation of Special Functions*, A Wiley-Interscience publication (Wiley, 1996).
- [80] L. A. Harland-Lang, V. A. Khoze, and M. G. Ryskin, “Exclusive LHC physics with heavy ions: SuperChic 3,” *Eur. Phys. J.* **C79**, 39 (2019), [arXiv:1810.06567 \[hep-ph\]](#).
- [81] T. Sjostrand, S. Mrenna, and P. Z. Skands, “A Brief Introduction to PYTHIA 8.1,” *Comput. Phys. Commun.* **178**, 852–867 (2008), [arXiv:0710.3820 \[hep-ph\]](#).
- [82] J. de Favereau, C. Delaere, P. Demin, A. Giammanco, V. Lemaître, A. Mertens, and M. Selvaggi (DELPHES 3), “DELPHES 3, A modular framework for fast simulation of a generic collider experiment,” *JHEP* **02**, 057 (2014), [arXiv:1307.6346 \[hep-ex\]](#).
- [83] Morad Aaboud *et al.* (ATLAS), “Performance of the ATLAS Trigger System in 2015,” *Eur. Phys. J.* **C77**, 317 (2017), [arXiv:1611.09661 \[hep-ex\]](#).
- [84] ATLAS Collaboration, *The ATLAS Tau Trigger in Run 2*, Tech. Rep. ATLAS-CONF-2017-061 (2017).
- [85] ATLAS Collaboration, *Performance of the ATLAS Minimum Bias and Forward Detector Triggers in 2011 Heavy Ion Run*, Tech. Rep. ATLAS-CONF-2012-122 (2012).
- [86] ATLAS Collaboration, *Performance of the ATLAS Minimum Bias and Forward Detector Triggers in pPb collisions*, Tech. Rep. ATLAS-CONF-2013-104 (2013).
- [87] ATLAS Collaboration, *Zero degree calorimeters for ATLAS*, Tech. Rep. CERN-LHCC-2007-01 (2007).
- [88] ATLAS Collaboration, “Electron reconstruction and identification in the ATLAS experiment using the 2015 and 2016 LHC proton-proton collision data at $\sqrt{s} = 13$ TeV,” Submitted to: *Eur. Phys. J.* (2019), [arXiv:1902.04655 \[physics.ins-det\]](#).
- [89] ATLAS Collaboration, “Muon reconstruction performance of the ATLAS detector in proton-proton collision data at $\sqrt{s} = 13$ TeV,” *Eur. Phys. J.* **C76**, 292 (2016), [arXiv:1603.05598 \[hep-ex\]](#).
- [90] M. E. Pospelov and I. B. Khriplovich, “Electric dipole moment of the W boson and the electron in the Kobayashi-Maskawa model,” *Sov. J. Nucl. Phys.* **53**, 638–640 (1991), [*Yad. Fiz.* 53,1030(1991)].
- [91] D. Ng and J. N. Ng, “A Note on Majorana neutrinos, leptonic CKM and electron electric dipole moment,” *Mod. Phys. Lett.* **A11**, 211–216 (1996), [arXiv:hep-ph/9510306 \[hep-ph\]](#).
- [92] K. Inami *et al.* (Belle), “Search for the electric dipole moment of the tau lepton,” *Phys. Lett.* **B551**, 16–26 (2003), [arXiv:hep-ex/0210066 \[hep-ex\]](#).
- [93] CMS Collaboration, *Technical Proposal for MIP timing detector in the CMS Experiment Phase 2 Upgrade*, Tech. Rep. CERN-LHCC-2017-027 (2017).
- [94] W. Yu (ALICE), “Particle identification of the ALICE TPC via dE/dx ,” *Nucl. Instrum. Meth.* **A706**, 55–58 (2013).

Appendix A: Simulation validation

We present additional material to validate the technical implementation of our simulation setup models the intended physics effects within the scope of our work. This includes the photon flux we implemented in MADGRAPH 2.6.5 [74, 75], and the interface with SMEFTSIM [72] for BSM modifications and interference with the SM.

Figure 4 displays generator level differential distributions of $p_T(\tau)$ for $\gamma\gamma \rightarrow \tau\tau$ considering various photon fluxes from protons and lead (Pb) beams. The distribution generated in MADGRAPH with Pb uses our custom implementation of Pb ion photon flux. We validate this with the corresponding distribution generated in SUPERCHIC 3.02 [80]. The latter includes a full treatment of nuclear effects that are neglected by the factorized prescription in MADGRAPH. These two distributions are in reasonable agreement for the scope of our work. Also shown are the corresponding distributions for proton beams. This illustrates that the impact of a nucleus with comparatively finite size is to soften the $p_T(\tau)$ spectrum compared to using proton beams.

Figure 5 shows the impact of the interference behavior on the inclusive cross-sections of $\sigma_{\gamma\gamma \rightarrow \tau\tau}^{(PbPb)}$ for coupling variations δa_τ using SMEFTSIM. We account for the interference between SM and BSM $\gamma\gamma \rightarrow \tau\tau$ diagrams in the matrix element \mathcal{M} squared

$$|\mathcal{M}|^2 = \left| \mathcal{M}_{\text{SM}} + \mathcal{M}_{\text{BSM}}^{(1)} + \mathcal{M}_{\text{BSM}}^{(2)} \right|^2 \quad (\text{A1})$$

$$= \left| \begin{array}{c} \text{diagram 1} \\ \text{diagram 2} \\ \text{diagram 3} \end{array} \right|^2. \quad (\text{A2})$$

A BSM coupling is represented by \bullet in the matrix element diagrams. Cross-sections featuring just the diagrams with only 1 BSM coupling (blue triangle) and only 2 BSM couplings (blue square) are shown in Fig. 5, which correspond to the amplitudes $\mathcal{M}_{\text{BSM}}^{(1)}$ and $\mathcal{M}_{\text{BSM}}^{(2)}$ respectively. As δa_τ deviates from zero in the negative direction, $\sigma_{\gamma\gamma \rightarrow \tau\tau}^{(PbPb)}$ falls to a minimum at $\delta a_\tau \simeq -0.04$ due to destructive interference from $\mathcal{M}_{\text{BSM}}^{(1)}$. Then, the constructively interfering $\mathcal{M}_{\text{BSM}}^{(2)}$ term begins to dominate for more negative δa_τ values and $\sigma_{\gamma\gamma \rightarrow \tau\tau}^{(PbPb)}$ rises again.

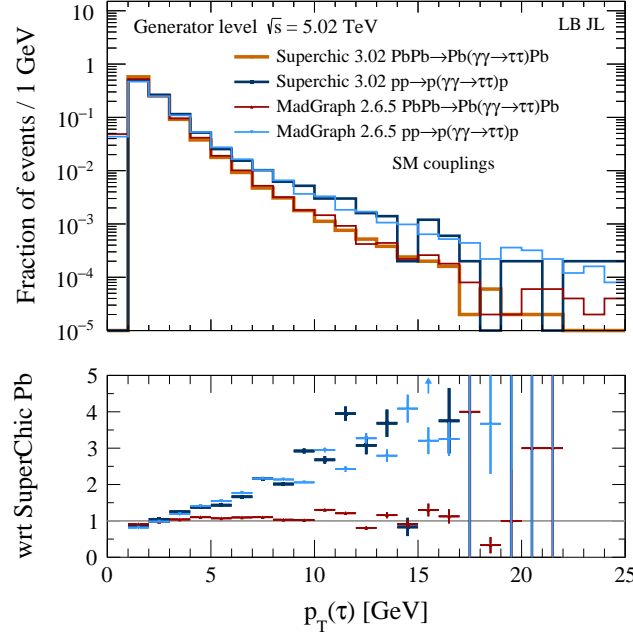


FIG. 4. Unit normalized generator level tau p_T distributions for $\gamma\gamma \rightarrow \tau\tau$ using SM couplings. These are generated in SUPERCHIC 3.02, which includes a full treatment of nuclear effects for lead (Pb) ions (orange). Also shown is the corresponding sample with protons (dark blue). The MADGRAPH 2.6.5 samples uses a factorized photon flux prescription for protons (light blue) and our implementation of Pb ion flux (red). The ratio panel is with respect to the SUPERCHIC Pb ions sample.

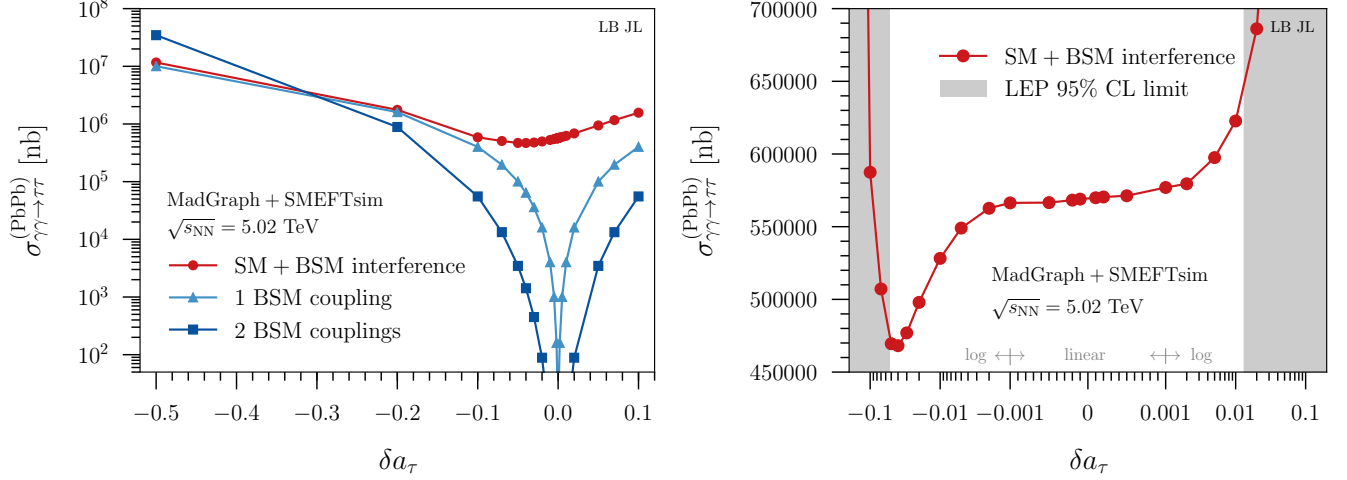


FIG. 5. Generator level cross-sections for $\gamma\gamma \rightarrow \tau\tau$ sourced by our implementation of the Pb photon flux in MADGRAPH. This is interfaced with SMEFTsim for BSM coupling variations in δa_τ defined in Eq. 4 of the main text, fixing $\delta d_\tau = 0$ at $\sqrt{s_{NN}} = 5.02$ TeV. Left shows the contribution from only 1 BSM coupling (light blue triangles), 2 BSM couplings (dark blue squares), and their combined interference with the SM (red circles). The markers indicate the sampled points from δa_τ . Right zooms in to the δa_τ values near zero with gray regions denoting the 95% CL exclusion by DELPHI, where the horizontal axis is linear scale for $\delta a_\tau \in [-0.001, 0.001]$ and logarithmic elsewhere.

Appendix B: Cutflows and χ^2 distributions

We provide technical material supporting the results presented in the main text. These include signal and background counts after sequentially applying kinematic requirements (cutflow), and χ^2 distributions as functions of δa_τ and δd_τ used to derive the final constraints.

Requirement	$\tau\tau$ (0,0)	$\tau\tau$ (0.005,0)	$\tau\tau$ (-0.01,0)	$\mu\mu$	ee	bb	cc	ss	uu	dd
1 lepton + 1 track analysis (SR1 ℓ 1T)										
$\sigma \times \mathcal{L}$	1139800	1195060	1056400	844080	844080	2999	604080	37754	604080	37754
$\sigma \times \mathcal{L} \times \epsilon_{\text{filter}}$	241140	253920	226300	844080	844080	2999	604080	37754	604080	37754
1 ℓ plus 1 track	20492.2	21619.3	19348.4	263443	3299.3	5.4	2905.0	0.3	5.4	0.2
$p_T^{e/\mu} > 4.5/3$ GeV, $ \eta^{e/\mu} < 2.5/2.4$	3659.9	3882.7	3582.8	79043	3118.9	1.1	4.8	0.0	0.0	0.0
2 tracks, $p_T^{\text{trk}} > 0.5$ GeV, $ \eta^{\text{trk}} < 2.5$	3324.5	3535.9	3256.9	78973	3117.8	1.0	3.0	0.0	0.0	0.0
$ \Delta\phi(\ell, \text{trk}) < 3$	1519.7	1605.7	1468.3	0.9	5.3	0.7	1.8	0.0	0.0	0.0
$m_{\ell, \text{trk}} \notin \{[3, 3.2], [9, 11]\}$ GeV	1275.1	1353.6	1242.3	0.9	5.3	0.2	1.2	0.0	0.0	0.0
$p_T^\ell \leq 6.0$ GeV	1197.7	1262.3	1154.7	0.9	0.0	0.2	1.2	0.0	0.0	0.0
$p_T^\ell > 6.0$ GeV	77.3	91.3	87.6	0.0	5.3	0.0	0.0	0.0	0.0	0.0
1 lepton + multitrack analysis (SR1 ℓ 2/3T)										
$\sigma \times \mathcal{L}$	1139800	1195060	1056400	844080	844080	2999	604080	37754	604080	37754
$\sigma \times \mathcal{L} \times \epsilon_{\text{filter}}$	241140	253920	226300	844080	844080	2999	604080	37754	604080	37754
1 ℓ plus 2 or 3 tracks	5945.1	6260.1	5572.2	33.8	23.2	43.8	8056.6	5.4	132.9	6.8
$p_T^{e/\mu} > 4.5/3$ GeV, $ \eta^{e/\mu} < 2.5/2.4$	1010.0	1073.3	978.6	12.2	4.2	1.8	13.3	0.0	0.0	0.0
3 tracks, $p_T^{\text{trk}} > 0.5$ GeV, $ \eta ^{\text{trk}} < 2.5$	519.9	548.1	485.8	5.6	4.2	0.8	4.8	0.0	0.0	0.0
4 tracks, $p_T^{\text{trk}} > 0.5$ GeV, $ \eta ^{\text{trk}} < 2.5$	370.5	398.3	381.1	0.0	0.0	0.4	3.6	0.0	0.0	0.0

TABLE I. Cutflow of yields after each requirement applied sequentially, normalized to $\mathcal{L} = 2 \text{ nb}^{-1}$ for the different analyses. For the $\gamma\gamma \rightarrow \tau\tau$ signal processes, we show these for benchmark points with parameter values labeled by $(\delta a_\tau, \delta d_\tau)$ displayed in the column header. Backgrounds are shown for various dilepton $\mu\mu, ee$ and diquark where the letters denote the flavor. The initial value in each cutflow is the cross-section σ times luminosity \mathcal{L} , followed by the efficiency ϵ_{filter} of the filter applied at generator level to the $\gamma\gamma \rightarrow \tau\tau$ samples.

Table I presents the set of cutflows for the different analyses, sequentially displaying the yields normalized to 2 nb^{-1} after each signal region requirement. Three benchmark signals are shown for the $\gamma\gamma \rightarrow \tau\tau$ samples at the SM values $(\delta a_\tau, \delta d_\tau) = (0, 0)$ and for values near the threshold of 68% CL sensitivity $(\delta a_\tau, \delta d_\tau) \in \{(0.005, 0), (-0.01, 0)\}$.

Figure 6 shows the χ^2 distributions as a function of δa_τ and δd_τ assuming 10% systematics, 2 nb^{-1} to allow comparison of constraining power between the different analyses presented in the main text.

Figure 7 displays the combined $\chi^2 = \sum_i \chi_i^2$ distributions. The combined χ^2 distributions are shown for 10% systematics at 2 nb^{-1} together with prospects using 5% systematics and extrapolation to 20 nb^{-1} . The red lines show the results from combining the three track SRs. The final combined χ^2 for the results in the main text take the green lines, which combine all four signal regions (SR1 ℓ 1T is divided into two orthogonal p_T^ℓ bins). The final 68% CL and 95% CL intervals are defined by where the χ^2 distributions intersect with $\chi^2 = 1$ and $\chi^2 = 3.84$ respectively.

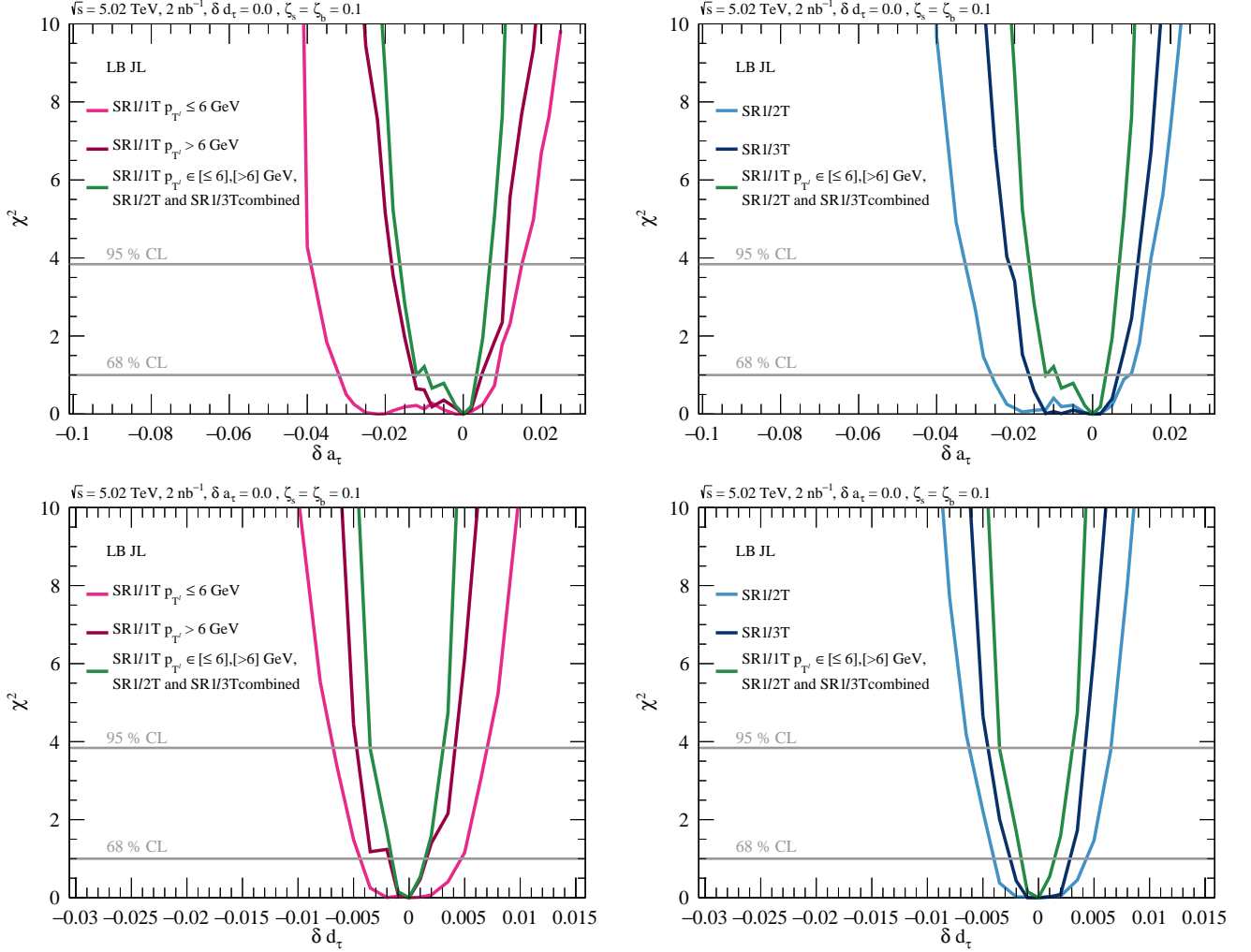


FIG. 6. The χ^2 distributions as a function of δa_τ assuming $\delta d_\tau = 0$ (upper), and δa_τ assuming $\delta d_\tau = 0$ (lower) are displayed for 10% systematics at $\mathcal{L} = 2 \text{ nb}^{-1}$. Left shows the results from the SR1 ℓ 1T regions and the impact of binning in p_T^ℓ . Right shows the results from the SR1/2/3T regions. The four signal region combined χ^2 is shown by the green line for reference. The gray horizontal lines correspond to 68% CL ($\chi^2=1$) and 95% CL ($\chi^2=3.84$)

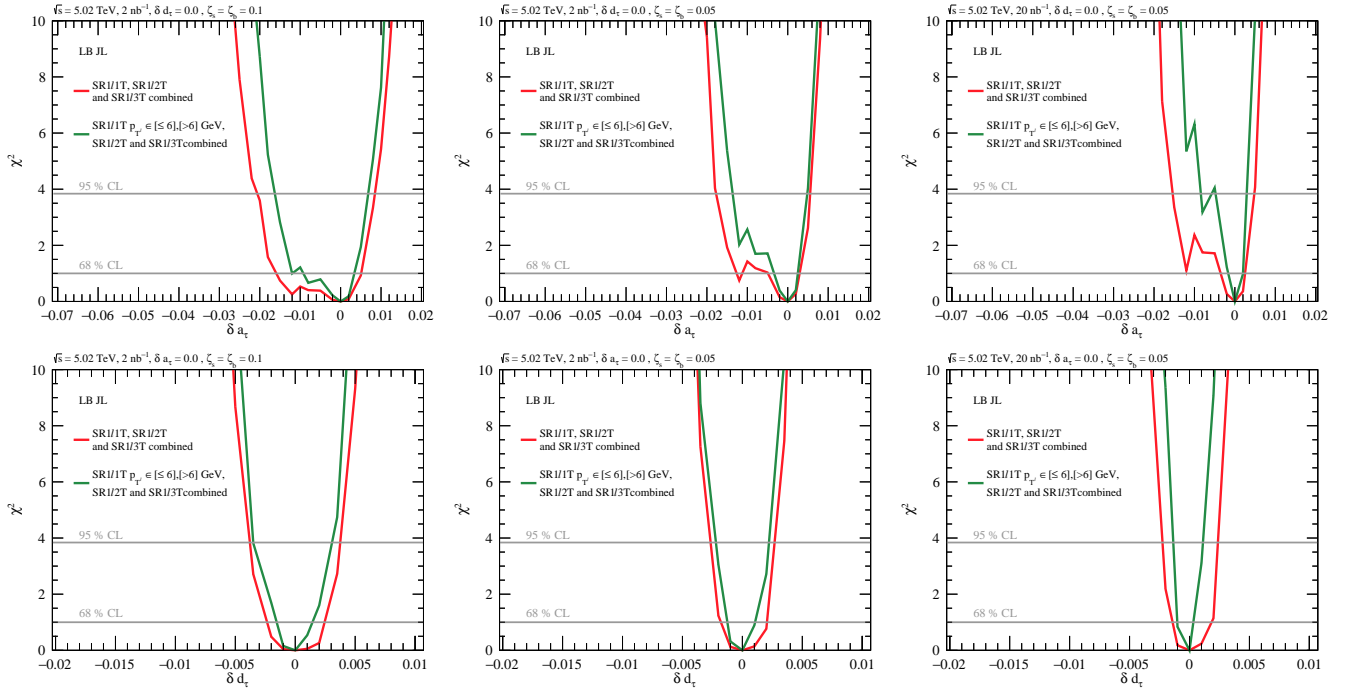


FIG. 7. The χ^2 distributions as a function of δa_τ assuming $\delta d_\tau = 0$ (upper), and δa_τ assuming $\delta d_\tau = 0$ (lower). These are displayed for 10% (left), 5% (centre) systematics at $\mathcal{L} = 2 \text{ nb}^{-1}$, and 5% systematics result extrapolated to $\mathcal{L} = 20 \text{ nb}^{-1}$ (right). The combined χ^2 for all three track SRs is shown by the red line, while the impact of dividing SR1l1T into two orthogonal p_T bins is shown by the green line. The gray horizontal lines correspond to 68% CL ($\chi^2=1$) and 95% CL ($\chi^2=3.84$)